

UNIVERSIDAD DE CONCEPCIÓN



CENTRO DE INVESTIGACIÓN EN
INGENIERÍA MATEMÁTICA (CI²MA)



High order approximation of mixed boundary value problems in
curved domains by extensions from polygonal subdomains

WEIFENG QIU, MANUEL SOLANO

PREPRINT 2015-06

SERIE DE PRE-PUBLICACIONES

HIGH ORDER APPROXIMATION OF MIXED BOUNDARY VALUE PROBLEMS IN CURVED DOMAINS BY EXTENSIONS FROM POLYGONAL DOMAINS

WEIFENG QIU * AND MANUEL SOLANO †

Abstract. This paper is a continuation of [*Solving Dirichlet boundary-value problems on curved domains by extensions from subdomains*, SIAM J. Sci. Comput. 34, pp. A497–A519 (2012)]. We generalize this technique of high order approximation of boundary value problems in curved domains with Dirichlet boundary data to the case of mixed boundary conditions. The treatment to Neumann boundary data is novel. We provide numerical results showing that, in order to obtain optimal high order convergence in this generalized setting, it is desirable to construct the computational domain by interpolating the boundary using piecewise linear segment. In this case the distance from the computational domain to the exact boundary is only $O(h^2)$.

Key words. discontinuous Galerkin, curved domains, high order, mixed boundary conditions

1. Introduction. In this paper we present a technique to numerically solve second order elliptic problems in domains Ω which are not necessarily polygonal. In particular we use a high order Hybridizable discontinuous Galerkin method (HDG) [3, 4] where the computational domain do not exactly fit the curved boundary. The main motivation of this technique is being able to use high order polynomial approximations and keep high order accuracy.

One of the first methods that approximate Neumann boundary conditions on curved domains considering non-fitted meshes was introduced by [1]. Here, a piecewise linear finite element method was considered and optimal convergence in the H^1 -norm was shown. In addition, the same authors solved a semi-definite Neumann problem on curved domains using a similar technique ([2]). In fact, they showed optimal behavior of the errors in H^1 and L^2 -norms using again piece-wise linear elements. On the other hand, higher order approximation finite element methods require to properly fit the boundary in order to keep high order accuracy. For instance, isoparametric element can be considered ([2],[11]). However these type of techniques are not practical specially in complicated geometries.

We proposed a more practical approach that considers unfitted meshes and it still preserves high order accuracy. One of the first ideas in this direction was introduced by [5] for the one-dimensional case and then extended to higher space dimensions for pure diffusion [9, 8] and convection-diffusion [9] equations. In addition, [7] applied this method to couple boundary element and HDG methods to solve exterior diffusion problems. However their work only considered Dirichlet boundary value problems because Neumann data can not be handled in the same way as we will explain below. The work presented here focuses on the treatment of part of the boundary where a Neumann data is prescribed.

We consider the following model problem defined in a general domain $\Omega \subset \mathbb{R}^2$

*Department of Mathematics, City University of Hong Kong, Hong Kong, email: weifeqiu@cityu.edu.hk. Partially supported by the GRF of Hong Kong (Grant No. 9041980 and 9042081).

†Corresponding author. Departamento de Ingeniería Matemática and CI²MA, Universidad de Concepción, Chile, email: msolano@ing-mat.udec.cl. Partially supported by CONICYT-Chile through grant FONDECYT-11130350, BASAL project CMM, Universidad de Chile and Centro de Investigación en Ingeniería Matemática (CI²MA).

with boundary Γ (not necessarily piecewise flat):

$$\begin{aligned}
(1.1a) \quad & -\nabla \cdot \mathbf{q} = f \text{ in } \Omega, \\
(1.1b) \quad & \mathbf{q} + \nabla u = 0 \text{ in } \Omega, \\
(1.1c) \quad & u = g_D \text{ on } \Gamma_D, \\
(1.1d) \quad & \mathbf{q} \cdot \mathbf{n} = g_N \text{ on } \Gamma_N.
\end{aligned}$$

Here Γ_D and Γ_N are the Dirichlet and Neumann part of Γ , respectively, such that $\Gamma_D \cap \Gamma_N = \emptyset$; $g_D \in H^{1/2}(\Gamma_D)$ and $g_N \in H^{-1/2}(\Gamma_N)$ are given data at the border and $f \in L^2(\Omega)$ is a source term.

We denote by D_h a polygonal domain that approximate Ω and not necessarily fit its boundary. We also assume that the computational boundary, Γ^h , satisfies $\Gamma^h = \Gamma_D^h \cap \Gamma_N^h$ and $\Gamma_D^h \cap \Gamma_N^h = \emptyset$ where Γ_D^h and Γ_N^h are part of Γ^h with Dirichlet (\tilde{g}_D) and Neumann (\tilde{g}_N) data, respectively. Thus, (1.1) can be written in D_h as follows:

$$\begin{aligned}
(1.2a) \quad & -\nabla \cdot \mathbf{q} = f \text{ in } D_h, \\
(1.2b) \quad & \mathbf{q} + \nabla u = 0 \text{ in } D_h, \\
(1.2c) \quad & u = \tilde{g}_D \text{ on } \Gamma_D^h, \\
(1.2d) \quad & \mathbf{q} \cdot \mathbf{n} = \tilde{g}_N \text{ on } \Gamma_N^h.
\end{aligned}$$

Here \tilde{g}_D and \tilde{g}_N are unknowns. As we mentioned before, \tilde{g}_D can be calculated following [5, 9, 7], i.e.,

$$(1.3) \quad \tilde{g}_D(\mathbf{x}) := g_D(\bar{\mathbf{x}}) + \int_{\sigma(\mathbf{x})} \mathbf{q} \cdot \mathbf{m} \, ds,$$

where $\sigma(\mathbf{x})$, is a path starting at $\mathbf{x} \in \Gamma_D^h$ and ending at $\bar{\mathbf{x}} \in \Gamma_D$; and \mathbf{m} is the tangent vector to $\sigma(\mathbf{x})$. This expression comes from integrating (1.1b) along the path $\sigma(\mathbf{x})$ (see [9] for details).

In principle, any kind of numerical method using polygonal domains can be used to solve the equations in D_h . However, it is desirable to consider those methods where an accurate approximation of \mathbf{q} is obtained, since the boundary condition (1.3) depends on that flux. We also notice from (1.3) that the same idea will not work for \tilde{g}_N since a similar expression will involve derivatives of \mathbf{q} which are not well approximated by the numerical method.

This paper is organized as follows. In Section 2 we give mesh construction and notation. In Section 3 we introduce the HDG method for curved domains with mixed boundary conditions where we explain the technique to handle the boundary data. In Section 4 we provide numerical results showing the performance of the method in different scenarios in order to determine the conditions needed to obtain optimal high order convergence. We end in Section 5 with concluding remarks.

2. Mesh construction and notation. We denote by h_K the diameter of the element $K \in D_h$ and by \mathbf{n} its outward unit normal. The meshsize h is defined as $\max_{K \in D_h} h_K$. Let \mathcal{E}_h^0 be the set of interior edges of D_h and \mathcal{E}_h^∂ the edges at the boundary. We say that an edge $e \in \mathcal{E}_h^0$ if there are two elements K^+ and K^- in D_h such that $e = \partial K^+ \cap \partial K^-$. Also, we say that $e \in \mathcal{E}_h^\partial$ if there is an element $K \in D_h$ such that $e = \partial K \cap \Gamma^h$. We set $\mathcal{E}_h = \mathcal{E}_h^0 \cup \mathcal{E}_h^\partial$.

For each element K in the triangulation D_h , we denote by $\mathcal{P}^k(K)$ the space of polynomials of degree at most k defined on the element K . For each edge e in

\mathcal{E}_h $\mathcal{P}^k(e)$ is the space of polynomials of degree at most k defined on the edge e . Given an element K , $(\cdot, \cdot)_K$ and $\langle \cdot, \cdot \rangle_{\partial K}$ denote the $L^2(K) = \{v : \int_K v^2 < \infty\}$ and $L^2(\partial K) = \{\xi : \int_{\partial K} \xi^2 < \infty\}$ products, respectively. Thus, for each ξ and ψ we define

$$(\xi, \psi)_{\mathcal{D}_h} = \sum_{K \in \mathcal{D}_h} (\xi, \psi)_K \quad \text{and} \quad \langle \xi, \psi \rangle_{\partial \mathcal{D}_h} = \sum_{K \in \mathcal{D}_h} \langle \xi, \psi \rangle_{\partial K}.$$

We also denote by $d(\Gamma, \Gamma^h)$ the distance between Γ and Γ^h .

3. The HDG method.

3.1. Formulation. The method seeks an approximation $(\mathbf{q}_h, u_h, \hat{u}_h)$ of the exact solution $(\mathbf{q}, u, u|_{\mathcal{E}_h})$ in the space $\mathbf{V}_h \times W_h \times M_h$ given by

$$(3.1a) \quad \mathbf{V}_h = \{\mathbf{v} \in [L^2(\mathcal{D}_h)]^2 : \mathbf{v}|_K \in [\mathcal{P}^k(K)]^2 \quad \forall K \in \mathcal{D}_h\},$$

$$(3.1b) \quad W_h = \{w \in L^2(\mathcal{D}_h) : w|_K \in \mathcal{P}^k(K) \quad \forall K \in \mathcal{D}_h\},$$

$$(3.1c) \quad M_h = \{\mu \in L^2(\mathcal{E}_h) : \mu|_e \in \mathcal{P}^k(e) \quad \forall e \in \mathcal{E}_h\}.$$

It is defined by requiring that it satisfies the equations

$$(3.2a) \quad -(\mathbf{q}_h, \nabla w)_{\mathcal{D}_h} + \langle \hat{\mathbf{q}}_h \cdot \mathbf{n}, w \rangle_{\partial \mathcal{D}_h} = (f, w)_{\mathcal{D}_h}$$

$$(3.2b) \quad (\mathbf{q}_h, \mathbf{v})_{\mathcal{D}_h} - (u_h, \nabla \cdot \mathbf{v})_{\mathcal{D}_h} + \langle \hat{u}_h, \mathbf{v} \cdot \mathbf{n} \rangle_{\partial \mathcal{D}_h} = 0,$$

$$(3.2c) \quad \langle \mu, \hat{\mathbf{q}}_h \cdot \boldsymbol{\nu} \rangle_{\partial \mathcal{D}_h \setminus \Gamma^h} = 0,$$

$$(3.2d) \quad \langle \mu, \hat{u}_h \rangle_{\Gamma_D^h} = \langle \mu, g_D^h \rangle_{\Gamma_D^h},$$

$$(3.2e) \quad \langle \mu, \hat{\mathbf{q}}_h \rangle_{\Gamma_N^h} = \langle \mu, g_N^h \rangle_{\Gamma_N^h},$$

for all $(\mathbf{v}, w, \mu) \in \mathbf{V}_h \times W_h \times M_h$. Here g_D^h is the approximation of \tilde{g}_D proposed by [9], i.e.,

$$(3.2f) \quad \tilde{g}_D(\mathbf{x}) \approx g_D^h := g_D(\bar{\mathbf{x}}) + \int_{\sigma(\mathbf{x})} \mathbf{q}_h \cdot \mathbf{m} \, ds,$$

where \mathbf{q}_h is a local extrapolation of the piecewise polynomial \mathbf{q}_h . On the other hand, g_N^h is an approximation of \tilde{g}_N which is still unknown. In Subsection 3.1.2 we propose to replace (3.2e) by an equation involving known quantities at the right hand side.

Finally, to complete the definition of the HDG method we must specify the definition of numerical trace $\hat{\mathbf{q}}_h$ on $\partial \mathcal{D}_h$, which we takes the form

$$(3.2g) \quad \hat{\mathbf{q}}_h = \mathbf{q}_h + \tau(u_h - \hat{u}_h)\mathbf{n}.$$

where τ is a positive stabilization parameter that guaranties solvability of (3.2) (ref. [3]).

3.1.1. Definition of the family of paths . The representation of g_D^h in (3.2f) is independent on the integration path. Let \mathbf{x} be a point on a boundary edge e . Previous work have proposed two ways to determine a point $\bar{\mathbf{x}}$ in Γ and hence construct $\sigma(\mathbf{x})$:

- (P1) If \mathbf{x} is a vertex, an algorithm developed by [9] uniquely determines $\bar{\mathbf{x}}$ as the closest point to \mathbf{x} such that $\sigma(\mathbf{x})$ does not intersect another path before terminating at Γ and does not intersect the interior of the domain Ω . In addition, if \mathbf{x} is not a vertex, its corresponding path is defined as convex combination of those paths associated to the vertices of e . For the Dirichlet boundary value problem, the authors in [9] numerically showed optimal rates of convergence with this choice of $\sigma(\mathbf{x})$ when $d(\Gamma, \Gamma^h)$ is of order h , that is, order $k+1$ for u_h and \mathbf{q}_h and order $k+2$ for the numerical trace \hat{u}_h .

(P2) On the other hand, [8] proposed to determine $\bar{\mathbf{x}}$ such that \mathbf{m} is normal to the edge e . In this case these authors theoretically proved that if $d(\Gamma, \Gamma^h)$ is of order h , the order of convergence for u_h and \mathbf{q}_h is indeed $k+1$, but the order for \hat{u}_h is only $k+3/2$. However, if $d(\Gamma, \Gamma^h)$ is of order $h^{5/4}$ the numerical trace also superconverges with order $k+2$. Moreover, they also showed numerical evidence indicating that the numerical trace optimally superconverges even though $d(\Gamma, \Gamma^h)$ is of order h .

Let now be e a boundary edge with vertices \mathbf{x}_1 and \mathbf{x}_2 . We denote by Γ_e the part of Γ determined by $\bar{\mathbf{x}}_1$ and $\bar{\mathbf{x}}_2$ as it is shown in Fig. 1. In this paper we assume that if $e \subset \Gamma_D^h(\Gamma_N^h)$ then $\Gamma_e \subset \Gamma_D(\Gamma_N)$. We point out that the algorithm in (P1) can be easily modified to satisfy this assumption. On the other hand, the paths defined in (P2) will not always satisfy this.

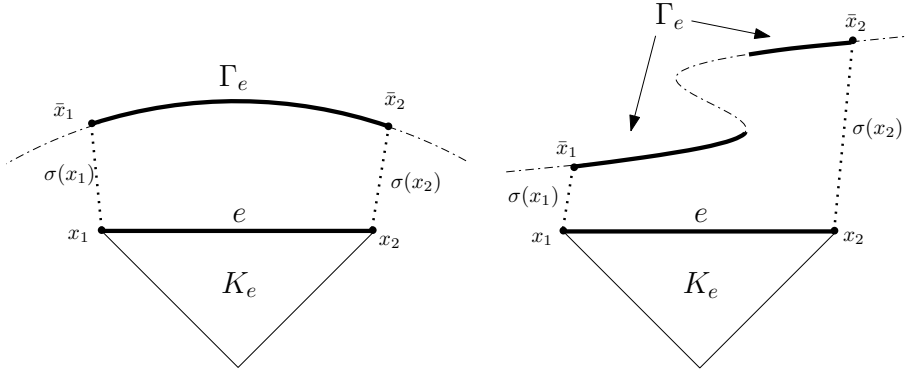


FIG. 1. Examples of a boundary edge e with vertices \mathbf{x}_1 and \mathbf{x}_2 . Γ_e is the segment of Γ_N determined by $\bar{\mathbf{x}}_1$ and $\bar{\mathbf{x}}_2$.

3.1.2. Approximation of the Neumann boundary condition. Let $e \subset \Gamma_N^h$ a Neumann boundary face and $\Gamma_e \subset \Gamma_N$ the part of Γ_N associated to e . We denote by K_e the element of the triangulation where e belongs. Then, $\mathbf{q}_h|_{K_e} \in [\mathcal{P}_k(K_e)]^2$ is extrapolated to Γ_e and the equation (3.2e) is replaced by imposing the following condition over \mathbf{q}_h :

$$(3.3) \quad \langle \mathbf{q}_h \cdot \mathbf{n}, \mu \rangle_{\Gamma_e} = \langle g_N, \mu \rangle_{\Gamma_e} \quad \forall \mu \in M(\Gamma_e),$$

where $M(\Gamma_e) := \{(\mathbf{p} \cdot \mathbf{n})|_e : \mathbf{p} \in [\mathcal{P}_k(\mathbb{R}^2)]^2\}$.

In order to implement (3.3), we assume that Γ_e can be parameterized by $s(t)$ with $t \in [0, 1]$. Hence (3.3) becomes

$$(3.4) \quad \int_0^1 (\mathbf{q}_h \cdot \mathbf{n})(\sigma(t)) \tilde{\mu} \|s'(t)\|_2 = \int_0^1 g_N(\sigma(t)) \tilde{\mu} \|s'(t)\|_2 \quad \forall \tilde{\mu} \in \widetilde{M}([0, 1]),$$

where $\widetilde{M}([0, 1]) = \mathbb{P}_k([0, 1])$.

4. Numerical results. In this section we present numerical experiments showing the performance the method. We measure the errors $e_u := u - u_h$, $e_q := \mathbf{q} - \mathbf{q}_h$

and $e_{\hat{u}} := u - \hat{u}_h$ by using the following norms:

$$\begin{aligned} \|e_u\|_{\text{int}} &:= \frac{\|e_u\|_{L^2(\mathcal{D}_h)}}{|\mathcal{D}_h|^{1/2}}, \quad \|e_{\mathbf{q}}\|_{\text{int}} := \frac{\|e_{\mathbf{q}}\|_{[L^2(\mathcal{D}_h)]^2}}{|\mathcal{D}_h|^{1/2}}, \\ \|e_{\hat{u}}\|_{\varepsilon_h} &:= \left(\frac{\sum_{K \in \mathcal{D}_h} h_K \|P_{\partial} u - \hat{u}_h\|_{L^2(\partial K)}^2}{\sum_{K \in \mathcal{D}_h} h_k |\partial K|} \right)^{1/2}. \end{aligned}$$

In addition we compute an element-by-element postprocessing, denoted by u_h^* , of the approximate solution u_h , which provides a better approximation for the scalar variable when $k \geq 1$ ([6, 4]). Given an element K we construct $u_h^* = \bar{u}_h + \tilde{u}_h$ as the only function in $\mathcal{P}^{k+1}(K)$ such that

$$\bar{u}_h = \begin{cases} \frac{1}{n} \sum_{e \in \partial K} \hat{u}_h|_e & \text{if } k = 0, \\ \frac{1}{|K|} \int_K u_h dx & \text{if } k > 0, \end{cases}$$

and \tilde{u}_h is the polynomial in $\mathcal{P}_0^{k+1}(K)$ (set of functions in $\mathcal{P}^{k+1}(K)$ with mean zero) satisfying

$$(\nabla \tilde{u}_h, \nabla w)_K = -(\mathbf{q}_h, \nabla w)_K \quad \forall w \in \mathcal{P}^{k+1}(K).$$

In the purely diffusive case, this new approximation of u has been proven to converge with order $k+2$ for $k \geq 1$ when the domain is polyhedral ([6, 4]), and also when it has curved Dirichlet boundary ([9, 8]).

We set the stabilization parameter $\tau \equiv 1$ in all the experiments. In Subsection 4.1 we show that deteriorate convergence can happen if $d(\Gamma, \Gamma^h) = O(h)$. However, we will see in Subsection 4.2 that optimal convergence is obtained when $d(\Gamma, \Gamma^h) = O(h^2)$.

4.1. Computational domain at a distance $d(\Gamma, \Gamma^h) = O(h)$. In the following examples the computational domain is constructed in such a way that the distance $d(\Gamma, \Gamma^h)$ is of order h . Moreover, f , g_D and g_N are chosen in order that $u(x, y) = \sin(x) \sin(y)$ is solution the exact of (1.1).

4.1.1. Example 1. Our first example consist of approximating a squared domain $\Omega = (0, 1)$ by a squared subdomain satisfying $d(\Gamma, \Gamma^h) = O(h)$ as Fig. 2 shows. Let $\Gamma_N = \{x : x = 0\}$, $\Gamma_D = \partial\Omega \setminus \Gamma_N$ and the family of paths is computed according to **(P2)**.

In Table 1 we display the history of convergence for different polynomial degree ($k = 0, 1, 2$ and 3) and meshsizes ($h = 1/2, 1/4, 1/8, 1/16$ and $1/32$). We observe that the error of u and \mathbf{q} behaves optimally with convergence rate of order $k+1$. Moreover the error of numerical trace and postprocessed solution also converge with order $k+1$, which is not optimal for the standard HDG method on polygonal domains. Even though, the errors e_{u^*} are always small than e_u . We attribute this lack of superconvergence to the fact that the Neumann condition (3.3) is being imposed on \mathbf{q}_h and not on $\hat{\mathbf{q}}_h$ as in the standard HDG method.

4.1.2. Example 2. We now consider an annular domain $\Omega = \{(x, y) \in \mathbb{R}^2 : 14^2 < x^2 + y^2 < 20^2\}$ that is being approximated by a polygonal subdomain satisfying $d(\Gamma, \Gamma^h) = O(h)$ as shown in Fig. 3. We consider Neumann data in the outer boundary $\Gamma_N = \{(x, y) \in \mathbb{R}^2 : x^2 + y^2 = 20^2\}$ and Dirichlet data in the inner

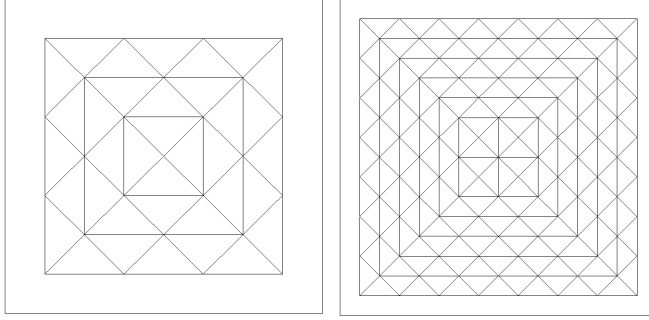


FIG. 2. Two consecutive meshes ($h = 1/4$ and $h = 1/8$) approximating the domain of Example 1. (Figure obtained from [8])

k	h	$\ e_u\ _{\text{int}}$		$\ e_q\ _{\text{int}}$		$\ e_{\bar{u}}\ _{\varepsilon_h}$		$\ e_{u^*}\ _{\text{int}}$	
		error	order	error	order	error	order	error	order
0	1/2	4.58E-03	-	6.59E-02	-	2.13E-02	-	7.50E-03	-
	1/4	6.09E-03	-0.41	4.77E-02	0.46	5.75E-03	1.89	6.60E-03	0.18
	1/8	4.62E-03	0.40	2.74E-02	0.80	1.75E-03	1.71	4.71E-03	0.49
	1/16	2.78E-03	0.73	1.46E-02	0.91	6.18E-04	1.51	2.80E-03	0.75
	1/32	1.52E-03	0.87	7.52E-03	0.96	2.51E-04	1.30	1.53E-03	0.88
1	1/2	1.54E-03	-	9.89E-03	-	3.70E-03	-	1.67E-03	-
	1/4	5.67E-04	1.44	2.55E-03	1.96	6.31E-04	2.55	4.68E-04	1.84
	1/8	1.69E-04	1.75	7.09E-04	1.85	1.50E-04	2.07	1.31E-04	1.83
	1/16	4.62E-05	1.86	1.94E-04	1.87	3.84E-05	1.97	3.60E-05	1.87
	1/32	1.21E-05	1.93	5.13E-05	1.92	9.83E-06	1.97	9.52E-06	1.92
2	1/2	2.29E-04	-	1.20E-03	-	5.23E-04	-	2.17E-04	-
	1/4	2.82E-05	3.02	1.24E-04	3.28	3.36E-05	3.96	2.44E-05	3.16
	1/8	3.43E-06	3.03	1.36E-05	3.19	3.22E-06	3.38	2.81E-06	3.12
	1/16	4.25E-07	3.01	1.63E-06	3.06	3.61E-07	3.16	3.38E-07	3.05
	1/32	5.28E-08	3.01	2.02E-07	3.01	4.26E-08	3.08	4.13E-08	3.03
3	1/2	3.37E-05	-	1.51E-04	-	7.55E-05	-	3.39E-05	-
	1/4	2.30E-06	3.87	9.32E-06	4.02	3.12E-06	4.59	2.30E-06	3.88
	1/8	1.55E-07	3.89	6.74E-07	3.79	1.78E-07	4.14	1.55E-07	3.89
	1/16	1.05E-08	3.89	4.76E-08	3.82	1.12E-08	3.99	1.05E-08	3.89
	1/32	6.90E-10	3.92	3.22E-09	3.89	7.13E-10	3.97	6.90E-10	3.92

TABLE 1
History of convergence of the approximation in Example 1.

boundary $\Gamma_D = \{(x, y) : x^2 + y^2 = 14^2\}$. Here the paths are computed according to **(P2)**.

The behavior of the L^2 -norm of the error displayed in Table 2 is similar to the one obtained in the previous example, i.e., the rate of convergence of the error in all the variables is of order $k + 1$. Thus, this example suggests that our technique performs properly when the boundary is actually non-polygonal.

4.1.3. Example 3. The numerical evidence provided in Examples 1 and 2 indicates that the technique proposed in this paper provides optimal rate of convergence when $d(\Gamma, \Gamma^h) = O(h)$ and the family of paths is constructed according to **(P2)**. However, in practice, this condition over the distance can not be satisfied in general, unless the mesh is constructed properly to do so.

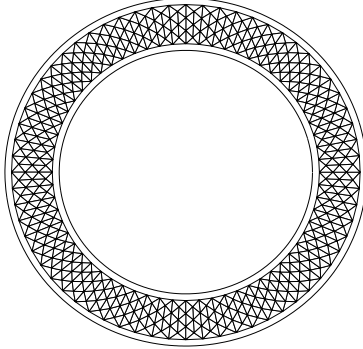


FIG. 3. Annular domain and mesh in Example 2.

k	h	$\ e_u\ _{\text{int}}$		$\ e_q\ _{\text{int}}$		$\ e_{\bar{u}}\ _{\mathcal{E}_h}$		$\ e_{u^*}\ _{\text{int}}$	
		error	order	error	order	error	order	error	order
0	1.89	9.56E+00	-	8.79E+00	-	4.66E-01	-	9.80E+00	-
	0.96	8.47E+00	0.18	5.82E+00	0.61	3.72E-01	0.33	8.50E+00	0.21
	0.49	5.72E+00	0.57	3.38E+00	0.79	2.42E-01	0.63	5.72E+00	0.56
	0.24	3.29E+00	0.81	1.82E+00	0.90	1.37E-01	0.83	3.29E+00	0.81
	0.12	1.76E+00	0.91	9.42E-01	0.91	7.26E-02	0.92	1.76E+00	0.91
1	1.89	2.03E+01	-	7.85E+00	-	9.56E-01	-	2.04E+01	-
	0.96	5.94E+00	1.82	2.12E+00	1.94	2.58E-01	1.94	5.96E+00	1.82
	0.49	1.43E+00	2.08	5.03E-01	2.10	6.00E-02	2.13	1.43E+00	2.08
	0.24	3.40E-01	2.09	1.20E-01	2.08	1.40E-02	2.11	3.40E-01	2.09
	0.12	8.19E-02	2.06	2.92E-02	2.06	3.35E-03	2.11	8.20E-02	2.06
2	1.89	4.04E+00	-	1.82E+00	-	1.90E-01	-	4.04E+00	-
	0.96	6.80E-01	2.64	3.42E-01	2.46	2.95E-02	2.76	6.81E-01	2.64
	0.49	1.41E-01	2.30	5.86E-02	2.58	5.89E-03	2.36	1.41E-01	2.30
	0.24	2.12E-02	2.75	8.33E-03	2.83	8.75E-04	2.77	2.12E-02	2.75
	0.12	2.88E-03	2.89	1.10E-03	2.93	1.16E-04	2.90	2.88E-03	2.93
3	1.89	4.12E+00	-	1.52E+00	-	1.93E-01	-	4.12E+00	-
	0.96	3.17E-01	3.80	1.07E-01	3.93	1.37E-03	3.92	3.17E-01	3.80
	0.49	1.89E-02	4.13	6.29E-03	4.15	7.89E-04	4.18	1.89E-02	4.13
	0.24	1.10E-03	4.13	3.70E-04	4.12	4.53E-05	4.15	1.10E-03	4.13
	0.12	6.56E-05	4.08	2.23E-05	4.07	2.68E-06	4.09	6.56E-05	4.08

TABLE 2
History of convergence of the approximation in Example 2.

A practical construction of the computational domain D_h was described in [9]. It consists of “immersing” the domain in a Cartesian background mesh and set D_h as the union of all the elements that are completely inside of Ω as it is shown in Fig. 4. Here $d(\Gamma, \Gamma^h) = O(h)$. In this case it is not convenient to construct the paths according to **(P2)**. In fact, given a point $\mathbf{x} \in \mathcal{E}_h^\partial$ it might happen that $\bar{\mathbf{x}}$ is extremely far from \mathbf{x} , specially in parts of Γ where the domain is non-convex. That is why we use the procedure described in **(P1)** instead.

In order to observe the performance of the method in this new setting we consider

the ring $\Omega = \{(x, y) \in \mathbb{R}^2 : 0.25^2 < (x - 0.5)^2 + (y - 0.5)^2 < 1\}$ with $\Gamma_N = \{(x, y) \in \mathbb{R}^2 : x^2 + y^2 = 1\}$ and $\Gamma_D = \{(x, y) : x^2 + y^2 = 0.25^2\}$. In Fig. 5 we show a zoom at the upper-right corner of three consecutive meshes. We also plot the family paths from vertices and quadrature points on the boundary edges.

In Table 3 we display the history of convergence. Even though the method is still convergent, the rates deteriorate. For the Dirichlet boundary value problem this non-optimal behavior does not occur as [9] showed. So, it seems that for Neumann boundary data the family of paths needs to be build according to **(P2)**.

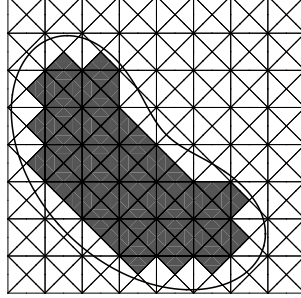


FIG. 4. Left: Domain Ω , its boundary Γ (solid line), a background mesh \mathcal{B}_h and the polygonal subdomain D_h (gray). Right: Dirichlet data g on Γ transferred to φ on Γ_h . (Figure taken from [9])

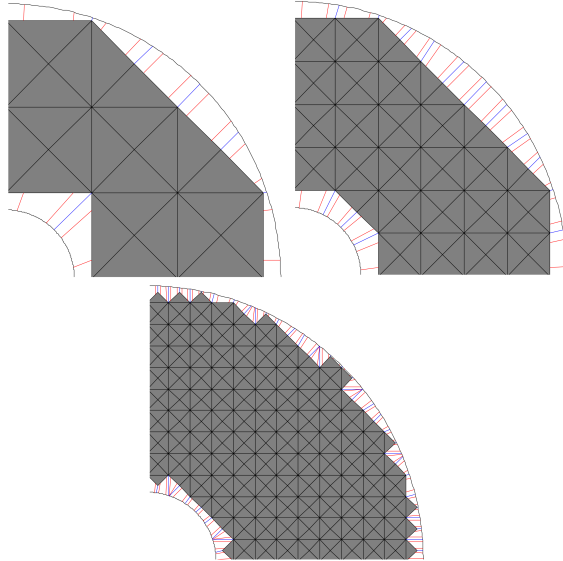


FIG. 5. Zoom at the upper-right corner of three consecutive meshes of Example 3. Mesh (grey region) constructed considering the procedure in [9] and family of paths determined according to **(P2)**. Blue lines: paths from the vertices. Red lines: paths from quadrature points of the boundary edges ($k = 1$).

4.2. Computational domain at a distance $d(\Gamma, \Gamma^h) = O(h^2)$. Another practical construction of D_h is defining first Γ^h by interpolating Γ using piecewise linear segments. Then, D_h is the domain enclosed by Γ_h as Fig. 6 shows. In this case $d(\Gamma, \Gamma_h) = O(h^2)$ and the family of paths can be easily defined according to **(P2)**.

k	h	$\ e_u\ _{\text{int}}$		$\ e_q\ _{\text{int}}$		$\ e_{\tilde{u}}\ _{\varepsilon_h}$		$\ e_{u^*}\ _{\text{int}}$	
		error	order	error	order	error	order	error	order
0	0.312	4.12E-02	-	1.83E-01	-	4.40E-02	-	4.15E-02	-
	0.156	3.70E-02	0.16	1.27E-01	0.53	3.26E-02	0.43	3.69E-02	0.17
	0.078	1.69E-02	1.13	1.37E-01	-0.11	1.50E-02	1.12	1.69E-02	1.13
	0.039	9.11E-03	0.89	7.00E-02	0.96	7.61E-03	0.97	9.11E-03	0.89
	0.019	8.50E-03	0.10	4.92E-02	0.51	5.66E-03	0.43	8.50E-03	0.10
1	0.312	6.13E-03	-	1.82E-02	-	3.75E-03	-	5.71E-03	-
	0.156	3.44E-03	0.84	1.06E-02	0.77	2.18E-03	0.78	3.37E-03	0.76
	0.078	3.86E-03	-0.17	9.41E-03	0.18	2.36E-03	-0.11	3.86E-03	-0.20
	0.039	1.16E-03	1.74	2.68E-03	1.81	6.88E-04	1.78	1.16E-03	1.73
	0.019	5.17E-04	1.16	1.16E-03	1.20	3.04E-04	1.18	5.16E-04	1.16
2	0.312	4.68E-04	-	1.25E-03	-	3.03E-04	-	4.60E-04	-
	0.156	2.25E-04	1.06	5.89E-04	1.08	1.45E-04	1.06	2.24E-04	1.04
	0.078	1.21E-04	0.89	3.24E-04	0.86	7.39E-05	0.97	1.21E-04	0.89
	0.039	1.31E-05	3.20	3.60E-05	3.17	7.79E-06	3.25	1.31E-05	3.21
	0.019	2.63E-06	2.32	7.03E-06	2.35	1.54E-06	2.33	2.63E-06	2.32
3	0.312	3.02E-05	-	8.78E-05	-	1.98E-05	-	3.00E-05	-
	0.156	1.11E-05	1.44	3.45E-05	1.35	7.19E-06	1.45	1.10E-05	1.44
	0.078	1.65E-06	2.75	5.37E-06	2.67	1.01E-06	2.83	1.65E-06	2.75
	0.039	6.69E-06	-	1.53E-05	-	3.98E-06	-	6.70E-06	-
	0.019	8.03E-03	-	2.26E-02	-	4.73E-03	-	8.04E-03	-

TABLE 3
History of convergence of the approximation in Example 3.

4.2.1. Example 4. We consider the domain $\Omega = \{(x, y) \in \mathbb{R}^2 : 1 < (x - 0.5)^2 + (y - 0.5)^2 < 4\}$ with $\Gamma_N = \{(x, y) \in \mathbb{R}^2 : x^2 + y^2 = 1\}$ and $\Gamma_D = \{(x, y) : x^2 + y^2 = 4\}$. In Table 4 we observe again that the order of convergence in all the variables is $k + 1$. We point out that part of the computational domain is outside of Ω as it can be observed in the inner circle in Fig. 6. This was never the case in the examples provided by [9] and [8]. Thus, these results indicate that their technique also works when $\Omega^c \cap D_h \neq \emptyset$.

In Fig. 7 we show the approximated solution p_h considering $h = 1.10$ (left) and 0.55 (right) and using polynomials of degree $k = 0, 1$ and 2 . We clearly see an improvement either when the mesh is refined or the polynomial degree increases.

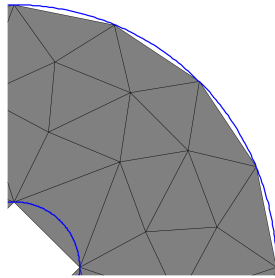


FIG. 6. Zoom at the upper-right corner of Example 4. Blue line: boundary Γ . Grey region: mesh.

4.2.2. Example 5. Now we test the performance of the method where Ω is a bounded domain exterior to an airfoil. This is the most difficult case in our examples since the domain has a boundary with a curved, re-entrant corner. The airfoil is

k	h	$\ e_u\ _{\text{int}}$		$\ e_q\ _{\text{int}}$		$\ e_{\hat{u}}\ _{\varepsilon_h}$		$\ e_{u^*}\ _{\text{int}}$	
		error	order	error	order	error	order	error	order
0	1.72	5.31E-01	-	2.14E+00	-	2.22E-01	-	6.63E-01	-
	1.10	2.87E-01	1.37	1.19E+00	1.3	1.14E-01	1.48	3.00E-01	1.77
	0.55	1.45E-01	0.99	6.13E-01	0.95	5.76E-02	1.00	1.46E-01	1.04
	0.29	8.10E-02	0.89	3.31E-01	0.95	3.10E-02	0.95	8.05E-02	0.91
	0.15	4.36E-02	0.98	1.69E-01	1.07	1.60E-02	1.05	4.34E-02	0.98
	0.08	2.24E-02	0.99	8.48E-02	1.02	8.12E-03	1.01	2.23E-02	1.00
1	1.72	2.59E-01	-	9.51E-03	-	9.51E-03	-	1.22E-01	-
	1.10	7.11E-02	2.89	1.61E-03	3.97	1.61E-03	3.97	1.80E-02	4.27
	0.55	1.77E-02	2.01	2.50E-04	2.68	2.50E-04	2.68	2.54E-03	2.82
	0.29	4.45E-03	2.12	5.92E-05	2.22	5.92E-05	2.22	4.23E-04	2.76
	0.15	1.08E-03	2.26	1.43E-05	2.25	1.43E-05	2.25	9.03E-05	2.45
	0.08	2.66E-04	2.08	4.24E-06	1.81	4.24E-06	1.81	2.69E-05	1.80
2	1.72	4.59E-02	-	6.22E-02	-	1.43E-03	-	1.04E-02	-
	1.10	6.55E-03	4.35	9.09E-03	4.29	1.95E-04	4.44	1.35E-03	4.56
	0.55	8.37E-04	2.97	1.26E-03	2.85	1.10E-05	4.15	8.25E-05	4.03
	0.29	1.12E-04	3.09	1.71E-04	3.07	2.14E-06	2.52	1.44E-05	2.67
	0.15	1.42E-05	3.29	2.11E-05	3.32	2.01E-07	3.75	1.34E-06	3.77
	0.08	1.77E-06	3.10	2.63E-06	3.10	3.37E-08	2.66	2.22E-07	2.68
3	1.72	5.61E-03	-	8.48E-03	-	.57E-04	-	1.28E-03	-
	1.10	4.47E-04	5.65	6.59E-04	5.71	6.52E-06	7.11	4.82E-05	7.32
	0.55	3.31E-05	3.75	4.77E-05	3.78	1.77E-07	5.20	1.42E-06	5.08
	0.29	2.26E-06	4.12	3.30E-06	4.11	1.51E-08	3.78	1.04E-07	4.01
	0.15	1.37E-07	4.46	2.12E-07	4.36	9.59E-10	4.39	6.42E-09	4.43
	0.08	8.47E-09	4.14	1.32E-08	4.13	9.52E-11	3.43	6.28E-10	3.46

TABLE 4

History of convergence of the approximation in Example 4.

obtained by using the Joukowski transformation:

$$J(z) = z + \frac{\lambda^2}{z},$$

where $z \in \mathbb{C}$ and $\lambda \in \mathbb{R}$. It is well known that this transformation maps the disc centered at (s_1, s_2) of radius R to an airfoil when we set $\lambda = R - \sqrt{s_1^2 + s_2^2}$. Here, we take $R = 0.1605$ and $s_1 = s_2 = 0.01$. In Fig. 8 we show three triangulations of the domain with meshsizes $h = 0.143, 0.073$ and 0.024 . Neumann boundary conditions are imposed around the airfoil and Dirichlet data in the remaining part of the boundary. We consider the following two examples:

- a) **Smooth solution.** We set f and g such that $u(x, y) = \sin(x) \sin(y)$ is the exact solution as in previous example. In Table 5 we observe that similar conclusions to those in previous examples can be drawn, even though in the case the domain is more complicated.
- b) **Non-smooth solution.** We now consider a potential flow around the airfoil where the exact solution in polar coordinates is $u(r, \theta) = r \cos(\theta) \left(1 + \frac{R^2}{r^2}\right)$. Here $g_N = 0$ around the airfoil. In this case ∇u has singularities at the leading and trailing edges, hence we do not expect high order convergence rates. In fact, this can be seen on Table 6 where in all the cases u converges with order one and q converges with order less than one. However, for a fixed mesh, the errors decrease when the polynomial degree increases. In Fig. 9 we

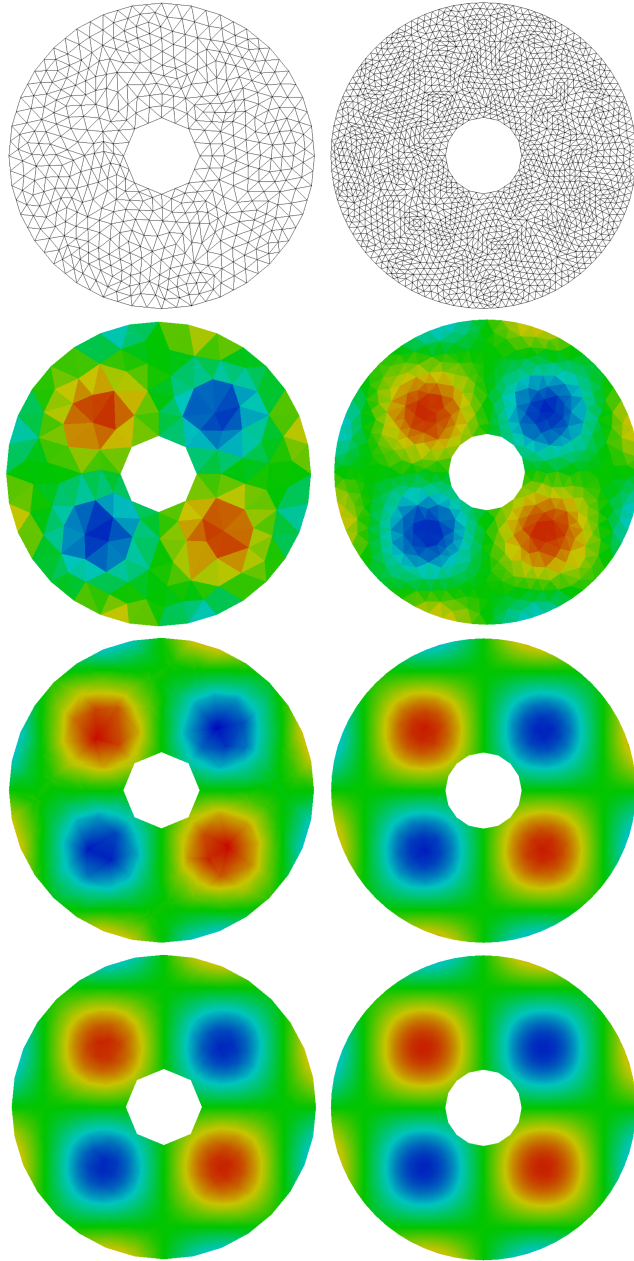


FIG. 7. Approximation of the scalar variable in Example 4. Columns: meshsize $h = 1.10$ and 0.55 . Rows: Polynomial of degree $k = 0, 1$ and 2 .

show the approximation of the x -component of \mathbf{q} considering $h = 0.143$ and 0.024 and $k = 0, 1$ and 2 .

5. Conclusions. We have proposed a technique for high order approximation of boundary value problems in curved domains with mixed boundary conditions. The main advantage of our approach is that the computational domain does not necessar-

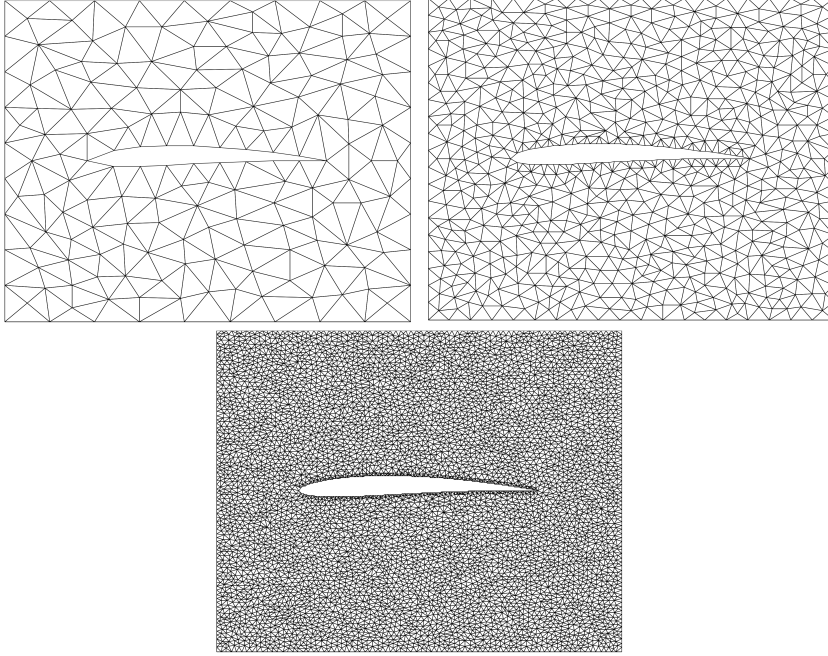


FIG. 8. Meshes of Example 5. Meshsizes $h = 0.143, 0.073$ and 0.024 .

k	h	$\ e_u\ _{\text{int}}$		$\ e_q\ _{\text{int}}$		$\ e_{\tilde{u}}\ _{\varepsilon_h}$		$\ e_{u^*}\ _{\text{int}}$	
		error	order	error	order	error	order	error	order
0	0.143	5.69E-03	-	2.25E-02	-	1.35E-03	-	5.76E-03	-
	0.113	4.78E-03	0.75	1.71E-02	1.18	7.52E-04	2.50	4.81E-03	0.77
	0.073	3.12E-03	0.98	1.05E-02	1.11	4.30E-04	1.29	3.14E-03	0.98
	0.038	1.59E-03	1.03	5.36E-03	1.04	1.97E-04	1.19	1.59E-03	1.04
	0.024	9.93E-04	1.02	3.25E-03	1.08	1.21E-04	1.06	9.94E-04	1.02
1	0.143	1.41E-04	-	2.91E-04	-	1.46E-05	-	1.48E-05	-
	0.113	8.04E-05	2.38	1.68E-04	2.33	8.36E-06	2.39	8.46E-06	2.37
	0.073	3.36E-05	2.01	6.72E-05	2.11	1.95E-06	3.35	1.96E-06	3.36
	0.038	8.51E-06	2.11	1.74E-05	2.07	5.30E-07	2.00	5.14E-07	2.05
	0.024	3.21E-06	2.11	6.50E-06	2.12	1.32E-07	3.00	1.28E-07	3.00
2	0.143	1.89E-06	-	3.58E-06	-	1.92E-07	-	1.85E-07	-
	0.113	8.56E-07	3.37	1.55E-06	3.56	6.58E-08	4.56	6.34E-08	4.56
	0.073	2.27E-07	3.06	4.06E-07	3.09	5.65E-09	5.65	5.67E-09	5.56
	0.038	2.96E-08	3.12	5.30E-08	3.12	6.17E-10	3.39	5.97E-10	3.45
	0.024	6.87E-09	3.15	1.24E-08	3.14	7.78E-11	4.47	7.57E-11	4.45
3	0.143	2.13E-08	-	3.00E-08	-	1.04E-08	-	9.98E-10	-
	0.113	7.16E-09	4.64	1.06E-08	4.44	3.33E-09	4.86	3.20E-10	4.85
	0.073	1.32E-09	3.89	1.80E-09	4.08	1.89E-10	6.61	1.83E-11	6.58
	0.038	8.65E-11	4.18	1.20E-10	4.14	1.47E-11	3.91	1.40E-12	3.95
	0.024	1.25E-11	4.17	1.75E-11	4.16	3.52E-12	3.09	3.32E-13	3.10

TABLE 5

History of convergence of the approximation in Example 5a) (smooth solution).

ily need to fit the boundary to be able to obtain high order accuracy. In particular, the novelty of this work is the treatment of the Neumann boundary data. We have

k	h	$\ e_u\ _{\text{int}}$		$\ e_q\ _{\text{int}}$		$\ e_{\tilde{u}}\ _{\varepsilon_h}$		$\ e_{u^*}\ _{\text{int}}$	
		error	order	error	order	error	order	error	order
0	0.143	2.49E-03	-	2.20E-02	-	1.40E-03	-	2.53E-0	-
	0.113	1.81E-03	1.35	1.62E-02	1.29	7.08E-04	2.92	1.84E-03	1.36
	0.073	1.11E-03	1.11	1.10E-02	0.90	2.94E-04	2.02	1.12E-03	1.14
	0.038	5.75E-04	1.01	7.23E-03	0.64	1.63E-04	0.91	5.77E-04	1.02
	0.024	3.49E-04	1.08	5.73E-03	0.50	9.09E-05	1.26	3.50E-04	1.08
1	0.143	4.04E-04	-	8.38E-03	-	4.29E-04	-	3.97E-04	-
	0.113	1.80E-04	3.45	5.60E-03	1.72	2.08E-04	3.09	1.89E-04	3.15
	0.073	7.93E-05	1.88	3.38E-03	1.16	8.83E-05	1.97	8.07E-05	1.96
	0.038	4.52E-05	0.86	2.00E-03	0.80	4.82E-05	0.93	4.53E-05	0.88
	0.024	3.03E-05	0.86	1.63E-03	0.45	3.23E-05	0.87	3.03E-05	0.87
2	0.143	1.55E-04	-	4.37E-03	-	1.77E-04	-	1.57E-04	-
	0.113	8.10E-05	2.78	3.02E-03	1.58	9.16E-05	2.81	8.12E-05	2.82
	0.073	4.91E-05	1.15	1.72E-03	1.30	5.35E-05	1.24	4.91E-05	1.16
	0.038	2.70E-05	0.92	9.71E-04	0.87	2.87E-05	0.95	2.70E-05	0.92
	0.024	1.70E-05	0.99	8.32E-04	0.33	1.81E-05	0.99	1.70E-05	0.99
3	0.143	7.94E-05	-	2.73E-03	-	9.13E-05	-	8.02E-05	-
	0.113	4.89E-05	2.06	1.84E-03	1.68	5.45E-05	2.19	4.92E-05	2.08
	0.073	3.59E-05	0.71	1.09E-03	1.21	3.90E-05	0.77	3.60E-05	0.72
	0.038	1.79E-05	1.07	6.34E-04	0.83	1.90E-05	1.10	1.79E-05	1.07
	0.024	1.07E-05	1.10	5.15E-04	0.45	1.14E-05	1.10	1.08E-05	1.10

TABLE 6

History of convergence of the approximation in Example 5b) (Non smooth solution).

provided numerical evidence suggesting that the technique performs properly if the family of paths is normal to the computational boundary. A practical way to always satisfy this restriction is to define Γ^h by interpolating Γ using piecewise linear segments. In this case distance to the exact boundary is $O(h^2)$.

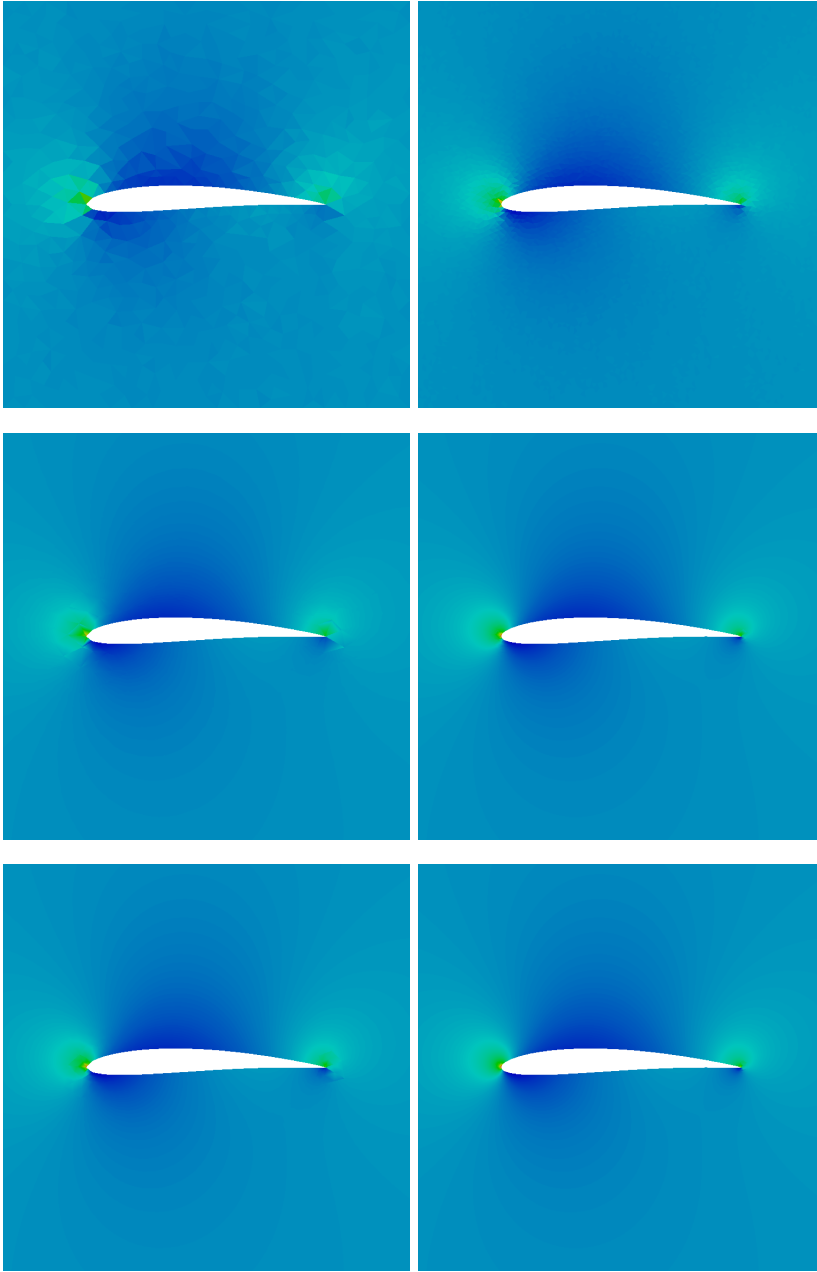


FIG. 9. Approximation of the x -component of \mathbf{q} Example 5 (non-smooth solution). Columns: meshsize $h = 0.143$ and 0.024 . Rows: Polynomial of degree $k = 0, 1$ and 2 .

REFERENCES

- [1] J.W. Barrett and C.M. Elliott, *A finite-element method for solving elliptic equations with Neumann data on a curved boundary using unfitted meshes*, IMA J. Numer. Anal., 4 (1984), pp. 309–325
- [2] J.W. Barrett and C.M. Elliott, *A practical finite element approximation of a semi-definite*

- Neumann problem on a curved domain*, Numer. Math., 51 (1987), pp. 23–36.
- [3] B. Cockburn, J. Gopalakrishnan and R. Lazarov, *Unified hybridization of discontinuous Galerkin, mixed and continuous Galerkin methods for second order elliptic problems*, SIAM J. Numer. Anal., 47 (2009), pp. 1319–1365.
 - [4] B. Cockburn, J. Gopalakrishnan and F.-J. Sayas, *A projection-based error analysis of HDG methods*, Math. Comp., 79 (2010), pp. 1351–1367.
 - [5] B. Cockburn, D. Gupta and F. Reitich, *Boundary-conforming discontinuous Galerkin methods via extensions from subdomains*, SIAM J. Sci. Comput., 42 (2010), pp. 144–184.
 - [6] B. Cockburn and J. Guzmán and H. Wang, *Superconvergent discontinuous Galerkin methods for second-order elliptic problems*, Math. Comp., 78 (2009), pp. 1–24.
 - [7] B. Cockburn, F.-J. Sayas, M. Solano, *Coupling at a Distance HDG and BEM*, SIAM J. Sci. Comput. 34, pp A28–A47 (2012).
 - [8] B. Cockburn, W. Qiu and M. Solano, *A priori error analysis for HDG methods using extensions from subdomains to achieve boundary-conformity*, Math. of Comp. 83, 286, pp. 665–699 (2014).
 - [9] B. Cockburn and M. Solano, *Solving Dirichlet boundary-value problems on curved domains by extensions from subdomains*, SIAM J. Sci. Comput. 34, pp. A497–A519 (2012).
 - [10] B. Cockburn and M. Solano, *Solving convection-diffusion problems on curved domains by extensions from subdomain*, J. Sci Comput. 59, 2, pp. 512–543 (2014).
 - [11] M. Lenoir, *Optimal isoparametric finite elements and errors estimates form domains involving curved boundaries*, SIAM J. Numer. Anal., 23 (1986), pp. 562–580.

Centro de Investigación en Ingeniería Matemática (CI²MA)

PRE-PUBLICACIONES 2014 - 2015

- 2014-30 JULIO ARACENA, LUIS GOMEZ, LILIAN SALINAS: *Complexity of limit cycle existence and feasibility problems in Boolean networks*
- 2014-31 RAIMUND BÜRGER, STEFAN DIEHL, THOMAS MAERE, INGMAR NOPENS, ELENA TORFS: *Impact on sludge inventory and control strategies using the Benchmark Simulation Model No. 1 with the Bürger-Diehl settler model*
- 2014-32 GABRIEL N. GATICA, LUIS F. GATICA, FILANDER A. SEQUEIRA: *Analysis of an augmented pseudostress-based mixed formulation for a nonlinear Brinkman model of porous media flow*
- 2014-33 JESSIKA CAMAÑO, RICARDO OYARZÚA, GIORDANO TIERRA: *Analysis of an augmented mixed-FEM for the Navier-Stokes problem*
- 2014-34 MARIO ÁLVAREZ, GABRIEL N. GATICA, RICARDO RUIZ-BAIER: *Analysis of a vorticity-based fully-mixed formulation for the 3D Brinkman-Darcy problem*
- 2014-35 JULIEN DESCHAMPS, ERWAN HINGANT, ROMAIN YVINEC: *From a stochastic Becker-Döring model to the Lifschitz-Slyozov equation with boundary value*
- 2015-01 SEBASTIAN DOMINGUEZ, GABRIEL N. GATICA, ANTONIO MARQUEZ, SALIM MEDDAHI: *A primal-mixed formulation for the strong coupling of quasi-Newtonian fluids with porous media*
- 2015-02 FELIPE LEPE, DAVID MORA, RODOLFO RODRÍGUEZ: *Finite element analysis of a bending moment formulation for the vibration problem of a non-homogeneous Timoshenko beam*
- 2015-03 FABIÁN FLORES-BAZÁN, FERNANDO FLORES-BAZÁN, CRISTIAN VERA: *Maximizing and minimizing quasiconvex functions: related properties, existence and optimality conditions via radial epiderivatives*
- 2015-04 RAIMUND BÜRGER, CHRISTOPHE CHALONS, LUIS M. VILLADA: *Antidiffusive Lagrangian-remap schemes for models of polydisperse sedimentation*
- 2015-05 ERNESTO CÁCERES, GABRIEL N. GATICA: *A mixed virtual element method for the pseudostress-velocity formulation of the Stokes problem*
- 2015-06 WEIFENG QIU, MANUEL SOLANO: *High order approximation of mixed boundary value problems in curved domains by extensions from polygonal subdomains*

Para obtener copias de las Pre-Publicaciones, escribir o llamar a: DIRECTOR, CENTRO DE INVESTIGACIÓN EN INGENIERÍA MATEMÁTICA, UNIVERSIDAD DE CONCEPCIÓN, CASILLA 160-C, CONCEPCIÓN, CHILE, TEL.: 41-2661324, o bien, visitar la página web del centro: <http://www.ci2ma.udec.cl>



**CENTRO DE INVESTIGACIÓN EN
INGENIERÍA MATEMÁTICA (CI²MA)
Universidad de Concepción**



Casilla 160-C, Concepción, Chile
Tel.: 56-41-2661324/2661554/2661316
<http://www.ci2ma.udec.cl>

